Geophys. J. Int. (2004) **159,** 1112–1124 doi: 10.1111/j.1365-246X.2004.02437.x

Viscoelastic–afterslip concurrence: a possible mechanism in the early post-seismic deformation of the M_w 7.6, 1999 Chi-Chi (Taiwan) earthquake

Shyh-Yang Sheu and Chiou-Fen Shieh

Institute of Seismology and Applied Geophysics, National Chung Cheng University, Chia-Yi, Taiwan. E-mail: seifent@eq.ccu.edu.tw

Accepted 2004 July 19. Received 2004 July 9; in original form 2003 July 15

SUMMARY

Observed coseismic data as well as 97 days of post-seismic GPS data for the Chi-Chi earthquake are used as constraints in the modelling of crustal evolution using the 3-D finite-element method. First, the coseismic GPS data are used to justify the use of the elastic earth model and the source rupture model. Subsequently, the most likely rheological model is determined by analysing several modelled time-dependent displacements for various viscosity structures. The range of viscosities of the lower crust in central Taiwan is determined in advance from laboratory measurements and the long-term strain rate. The estimated viscosity of 5.0×10^{17} Pa s seems to be very low and a relaxation time of 116 days seems very short, but the latter approximates the GPS measurement of 86 days. Since earlier studies have indicated that both the viscoelastic response model and the afterslip model may affect post-seismic deformation, we compare theoretical surface displacements for each of the two models that we evaluate. The results reveal that there is little doubt that while neither of these models alone is able to predict the GPS measurements well in a 97-day period, the combination of the two models improves the predictions considerably. We conclude that the afterslip mainly dominated Chi-Chi post-seismic deformation in the rupture area while the viscoelastic model did so elsewhere.

Key words: afterslip, Chi-Chi earthquake, crustal evolution, post-seismic deformation, viscoelastic response, viscosity.

1 INTRODUCTION

The M_w 7.6, 1999 Chi-Chi earthquake in central Taiwan which ruptured the north–south trending ChelungPu Fault (Fig. 1), was the most devastating in Taiwan in the twentieth century. The maximum horizontal displacement reached 10.1 m (Yu *et al.* 2001), while the total length of the surface rupture extended for about 100 km, mostly along the former fault scarp. Immediately after this major event, many additional GPS stations were installed in the source region and significant post-seismic deformation was observed for 97 days (Yu *et al.* 2001). This provided an invaluable data set with which to study the mechanism of early post-seismic deformation.

Two mechanisms have been postulated to explain early post-seismic deformation. The first is viscoelastic relaxation (Wahr & Wyss 1980), which produces large post-seismic displacements, and the other is afterslip (Marone *et al.* 1991) which produces aseismic creep in the epicentre area. The fundamental assumption behind the former mechanism is that a weak viscoelastic layer lies beneath a seismogenic zone which reloads the crust as it responds to coseismic stresses (Nur & Mavko 1974; Thatcher & Rundle 1984; Deng *et al.* 1998). Afterslip, on the other hand, assumes aseismic creep on the original fault plane, or the updip or downdip extension of the coseismic rupture plane, with the slip rate decreasing over time (Tse & Rice 1986; Marone *et al.* 1991). In this research, extensive modelling is conducted to identify the most realistic mechanisms involved in the early post-seismic deformation that occurred in Taiwan at the time of the Chi-Chi earthquake.

GPS measurements have clearly revealed broad-scale post-seismic deformation, especially on the hangingwall of the ChelungPu Fault. These data may indeed fit the transient state with a decaying relaxation time function of 86 days, as determined by Yu *et al.* (2001), and possibly they reflect a viscoelastic response (Shen *et al.* 1994; Ergintav *et al.* 2002). Since low Q values are generally associated with low viscosity (Wahr & Wyss 1980), the low Q values in western Taiwan (Wang 1993) have long led us to expect low viscosity there; this in turn corresponds to a short relaxation time. However, previous research has demonstrated that similar deformation is caused by either viscoelastic creep or afterslip (Rundle & Jackson 1977; Thatcher 1983; Savage 1990). Simply put, no single mechanism has ever been clearly distinguished. More recently Hsu *et al.* (2002) have reported that the early post-seismic deformation of the Chi-Chi event was caused mainly by afterslip. Nevertheless,

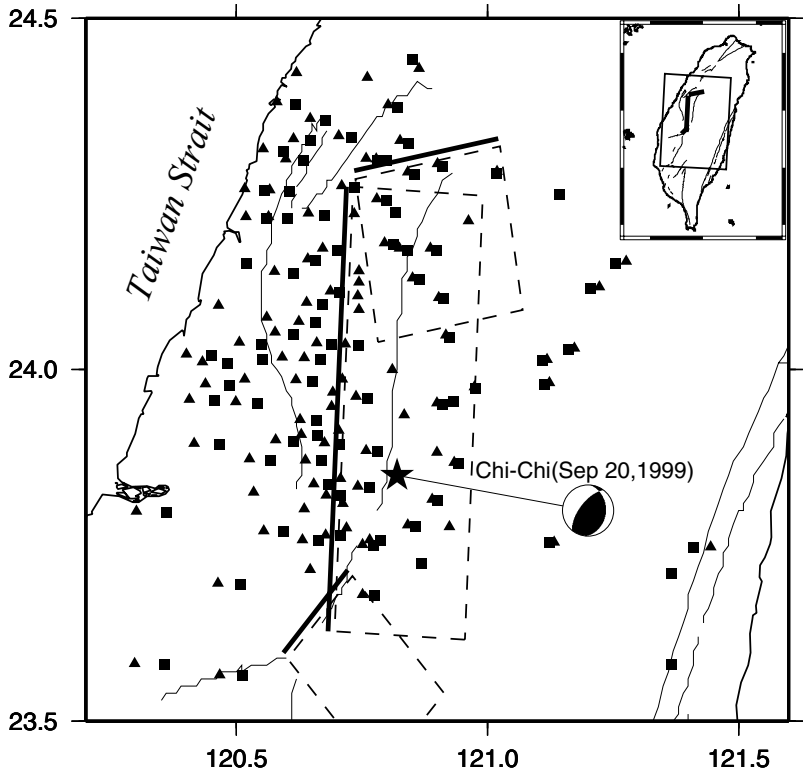

Figure 1. Map of central Taiwan showing the fault surface traces of the multiplane ChelungPu Fault (three heavy lines) and the surface projection of the fault planes (dashed rectangles) (Ji *et al.* 2001). The solid triangles and squares represent, respectively, the sites of the GPS stations set up before and after the Chi-Chi event. The epicentre of the Chi-Chi earthquake is marked with a star. The thin lines represent other active faults.

given the very short 86-day relaxation time (Yu *et al.* 2001), it begs the question of whether viscoelastic response is actually negligible or not. It is for these reasons that we decided that further investigation was required to identify and quantify the possible mechanisms that were involved in the post-seismic deformation of the 1999 Chi-Chi earthquake.

2 COMPUTATION OF TIME-DEPENDENT DISPLACEMENT

To effectively analyse post-seismic deformation, it is necessary to have a mathematical method and to define a layered earth model that contains a viscoelastic layer beneath a seismogenic zone. Although an analytic solution of static stress and displacement for a finite rectangular fault in an elastic half-space was developed by Chinnery (1961, 1963) and Okada (1985, 1992), it is not appropriate for a layered or viscoelastic medium. The differences between using a half-space model and a layered medium were reported by Cummins *et al.* (1998). In this present study, for the computation of deformation, we use both a 3-D finite-element method implemented in the software package (Deng *et al.* 1998) that is suitable for processing complicated boundary conditions and an inhomogeneous earth model (Melosh & Raefsky 1981; Yoshioka *et al.* 1989; Sato *et al.* 1996). The governing rheological equations are based on a non-Newtonian Maxwell constitutive relation (Melosh & Raefsky 1980).

To calculate displacement from a source rupture model with reasonable precision, central Taiwan (Fig. 1) is divided into a 50 × 41 × 30 finite mesh (using Cartesian coordinates), each mesh representing the length of the ChelungPu Fault in the N3°E (strike), E3°S and downward directions with lengths of 180, 140 and 72 km, respectively. The input earth model parameters are listed in Table 1 (see below for more details). The source model is adopted from Ji *et al.* (2001), and is constrained by GPS and strong motion data. At each artificial boundary of the finite meshes the displacement is set at zero, while at other nodes it is estimated under the condition that the system reaches equilibrium when the total potential energy is minimal (Zienkiewicz 1985). In other words, the top boundary of the model is a free surface, where displacements are calculated and compared with the observed GPS measurements. On the other five boundaries, the displacements are assumed to be zero (fixed boundary) in both horizontal and vertical directions.

Note that since the effect of gravity can be neglected in a short-term evolution it will not be included in our computation. The output includes coseismic displacement, $W(t_0)$, and time-dependent displacement, $W(t)$. The post-seismic deformation is then obtained from $\Delta W = W(t) - W(t_0)$ at time t. The time-dependent stress

Table 1. Elastic parameters of the central Taiwan region: Th is the thickness of the layer, E is Young's modulus and ν is Poisson's ratio.

Layer[a]	Th (km)	V_p (km s^{-1})	ρ (g cm^{-3})	E (10^{11} Pa)	ν
1	0.7	3.50	2.25	0.23	0.25
2	3.8	3.78	2.40	0.29	0.25
3	5.7	5.04	2.50	0.53	0.25
4	3.8	5.71	2.60	0.71	0.25
5	4.0	6.05	2.75	0.84	0.25
6	4.0	6.44	2.90	1.00	0.25
7	8.3	6.83	3.20	1.24	0.25
8	—	7.28	3.20	1.41	0.25

[a]Layer numbers correspond to numbers shown in Fig. 3.

changes are also included in the output but are not discussed in this study.

3 REGIONAL RHEOLOGICAL MODELS

Based on many observations, the rheological structure of central Taiwan consists of an elastic upper crust, a lower crust characterized as a Maxwell viscoelastic medium and the upper mantle. The upper crust behaves elastically (with a very long relaxation time) on timescales of 250–300 yr (Cohen 1982; Gardi *et al.* 2002), whereas the lower crust flows viscously (Freed & Lin 1998; Deng *et al.* 1999). The Moho discontinuity at a depth of 30.25 km was previously determined from 3-D velocity inversion (Ma *et al.* 1996). The boundary between the lower and upper crusts was determined from the concentration of 95 per cent of the aftershocks (Deng *et al.* 1999) occurring within 1 yr of the Chi-Chi event, as shown in Fig. 2. The aftershocks selected for the entire central Taiwan area with $M_L >$ 2.2 were concentrated above the boundary at a depth of 22 km, which closely approximates the 20 km obtained from the 3-D velocity inversion (Ma *et al.* 1996). The density value for each layer is adopted from the gravity modelling results of Yen *et al.* (1998), while Young's modulus is computed from the *P*-wave velocity structure of Ma *et al.* (1996) using the expression:

$$E = \frac{2}{3}(1+\nu)\rho\alpha^2, \tag{1}$$

where E is Young's modulus, ν is Poisson's ratio with a value of 0.25, ρ is density and α is *P*-wave velocity. All parameters for the layered model are listed in Table 1 for easy reference, and the three rheological models under investigation are illustrated in Fig. 3.

For the sake of simplification, the viscosity structure of the lower crust is usually assumed to be a flat layer, as shown in Fig. 3(a); in this study it is referred to as model A. Due to the complicated geological structure of Taiwan, which is located in an active mountain-building belt, the viscosity structure may not be as simple as that depicted in Fig. 3(a). Models B and C, shown in Figs 3(b) and (c), respectively, are two plausible alternative models. These are based on the lithosphere plate collision model of Taiwan (Wu *et al.* 1997), and both models assume that the central mountain range of Taiwan (see Fig. 3) is the product of crustal thickening due to the collision of the Philippine Sea and the Eurasian Continental plates. Model B assumes that the central mountains were formed by the uplifting of the crust in the absence of a mountain root, thus resulting in the flat Moho discontinuity. Model C assumes that a mountain root exists. The GPS data are compared with the modelling results for the three models (A, B and C) to help us identify which model is the most feasible.

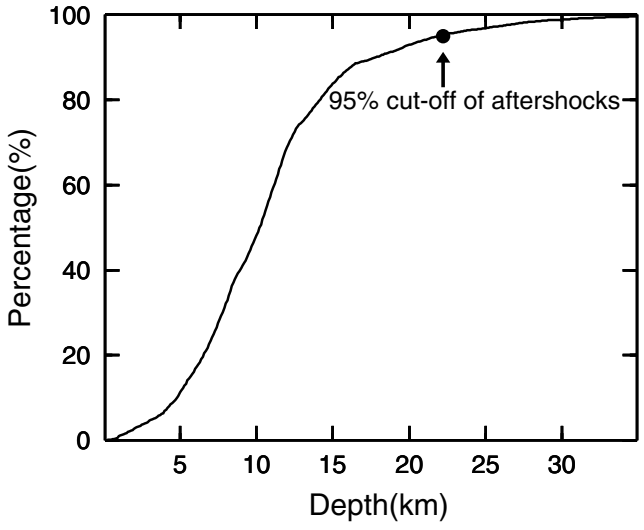

Figure 2. Distribution of the aftershocks in central Taiwan as a function of depth. The boundary between the lower and upper crusts is determined from the concentration of 95 per cent of the aftershocks of the Chi-Chi earthquake within 1 yr after the event. Most aftershocks (95 per cent) occurred above 22 km.

4 COSEISMIC DISPLACEMENTS

The horizontal coseismic displacements calculated for the Chi-Chi event, and model A (Fig. 3a) are illustrated in Fig. 4(a) (left) together with the GPS displacements. Note that the computed displacement at each finite-element node is bilinearly interpolated (Press *et al.* 1992) back to the location of each GPS station for clear visualization and easy comparison. For the most part, the patterns of the observed and calculated horizontal coseismic displacements are very similar, except for those in the northern part of the ChelungPu Fault where uncertainty in the rupture slip model is high (Ji *et al.* 2001). To estimate the consistency between the observed and calculated horizontal displacements, the correlation coefficient r is used to evaluate the statistical significance of the correlation, and is expressed as:

$$r = \frac{N\sum x_i y_i - \sum x_i \sum y_i}{\left[N\sum x_i^2 - \left(\sum x_i\right)^2\right]^{1/2}\left[N\sum y_i^2 - \left(\sum y_i\right)^2\right]^{1/2}}, \tag{2}$$

where x_i and y_i represent the observed and calculated values, respectively, and N is the number of data sets.

The correlations between the observed and predicted horizontal displacements in the east–west and north–south components are analysed separately in the scattergram shown in Fig. 4(a) (right). The correlation coefficient for the east–west component is 0.868, while that for the north–south component is similar at 0.894. The meaning of r (eq. 2) can be explained by the coefficient of determination, r^2, which indicates the percentage of data y_i that in turn can be explained by data x_i (Chase 1997). According to statistical decision theory, $r^2 > 70$ per cent ($r = 0.837$) is an acceptable test or prediction (Mulargia & Gasperini 1995; Papazachos & Papadimitriou 1997). We found that $r^2 = 0.80$ for the north–south component, or that 80 per cent of the observed GPS measurements are predicted by the calculated values. Similarly, for the east–west component we obtain a value of $r^2 = 0.753$ (75.3 per cent of the observed GPS measurements are predicted). Thus, the model fits the data in a statistically significant way. Coseismic uplift is the major feature in a thrust fault; however, surface subsidence can be observed near the surface projection of the down-dip edge of the fault (Cohen 1994). These phenomena are shown in Fig. 4(b) for our calculation. The coseismic uplift of the hangingwall decreases rapidly from west to east and becomes subsidence at PuLi town (solid triangle in Fig. 4b), which is confirmed by GPS measurement (Yu *et al.* 2001). Vertical components are not compared in this study on account of the high uncertainty in the GPS measurements (Yu *et al.* 2001). As coseismic displacement is an elastic response of the crust, the predicted displacements do not differ for the three models in Fig. 3, and it is therefore considered not necessary to show them.

5 ESTIMATION OF VISCOSITIES

The viscosity in the lower crust controls the time-dependent stress changes. One way to estimate the viscosity in the lower crust and

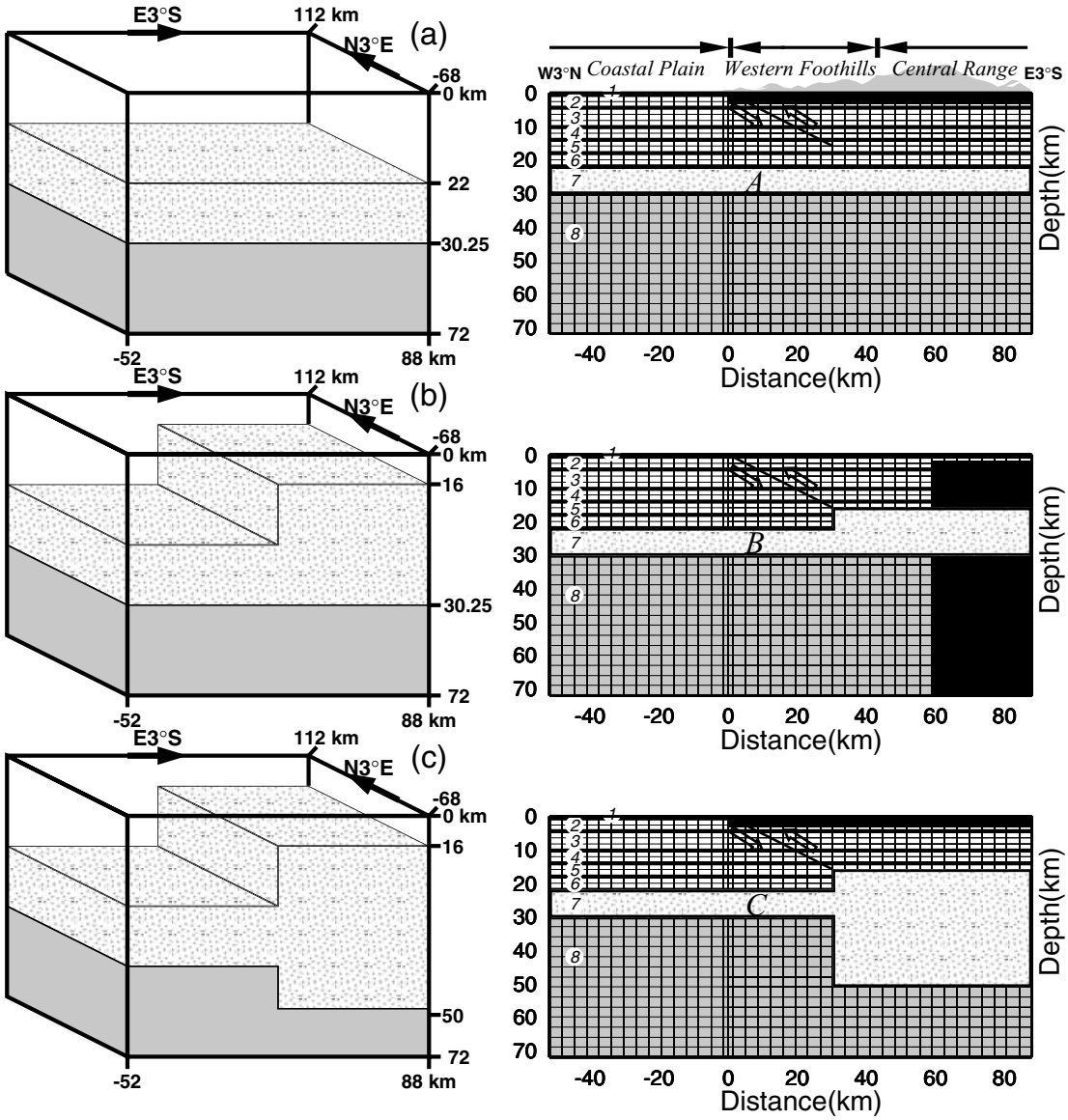

Figure 3. Model and cross-section of the 3-D finite-element meshes illustrating the viscosity volumes of lower crust (dotted areas) and upper mantle (grey areas) of the different models tested in this study. The numbers in the layers correspond to the material properties listed in Table 1. The 30° dipping line beneath the Western Foothills denotes the ChelungPu thrust fault. (a) A typical simplified viscosity layer in the lower crust. (b), (c) Alternative models based on the tectonics of central Taiwan (Wu *et al.* 1997).

upper mantle is to consider the creep parameters of many rock-forming minerals under both dry and wet conditions that were measured from laboratory experiments (Kirby & Kronenberg 1987), along with a long-term strain rate (Freed & Lin 1998) or the stress changes (Pollitz *et al.* 2000). Since the approximate range of viscosity can be estimated from surface deformation that has been observed within timescales of 1 month to 10 years (Sykes *et al.* 1999), the method that incorporated strain rate is used. Next, obtaining a minimum root mean square of intensive modelling results within the estimated range of viscosities is employed to determine the viscosities of lower crust and upper mantle. Despite the use of different parameters (or methods) which may result in different ranges of viscosities, the final realistic value is determined by grid search. The following descriptions explain the method.

The temperature as a function of depth within the Earth must be found in advance from the following expression (Turcotte & Schubert 2002).

$$T = T_0 + \frac{q_m z}{k} + \frac{(q_0 - q_m)h_r}{k}[1 - \exp(-z/h_r)] \quad (3)$$

where T_0 is surface temperature, q_0 is surface heat flux, q_m is the mantle heat flux, h_r is a length scale for the decrease in crustal radioactive element concentration with depth, k is the coefficient of thermal conductivity and z is the depth. In this study, the following set of parameters are used: $T_0 = 25°C$, $q_0 = 95$ mW m^{-2} (Barr & Dahlen 1989), $q_m = 30$ mW m^{-2}, $h_r = 10$ km and $k = 3.35$ W m^{-1} K^{-1} (Turcotte & Schubert 2002). For the realistic flow characteristic of rocks, the deviatoric stress, σ, is calculated based on a power law of the form (Kirby & Kronenberg 1987):

$$\sigma^n = \left(\frac{1}{A}\right)\hat{e}\exp\left(\frac{Q}{RT}\right) \quad (4)$$

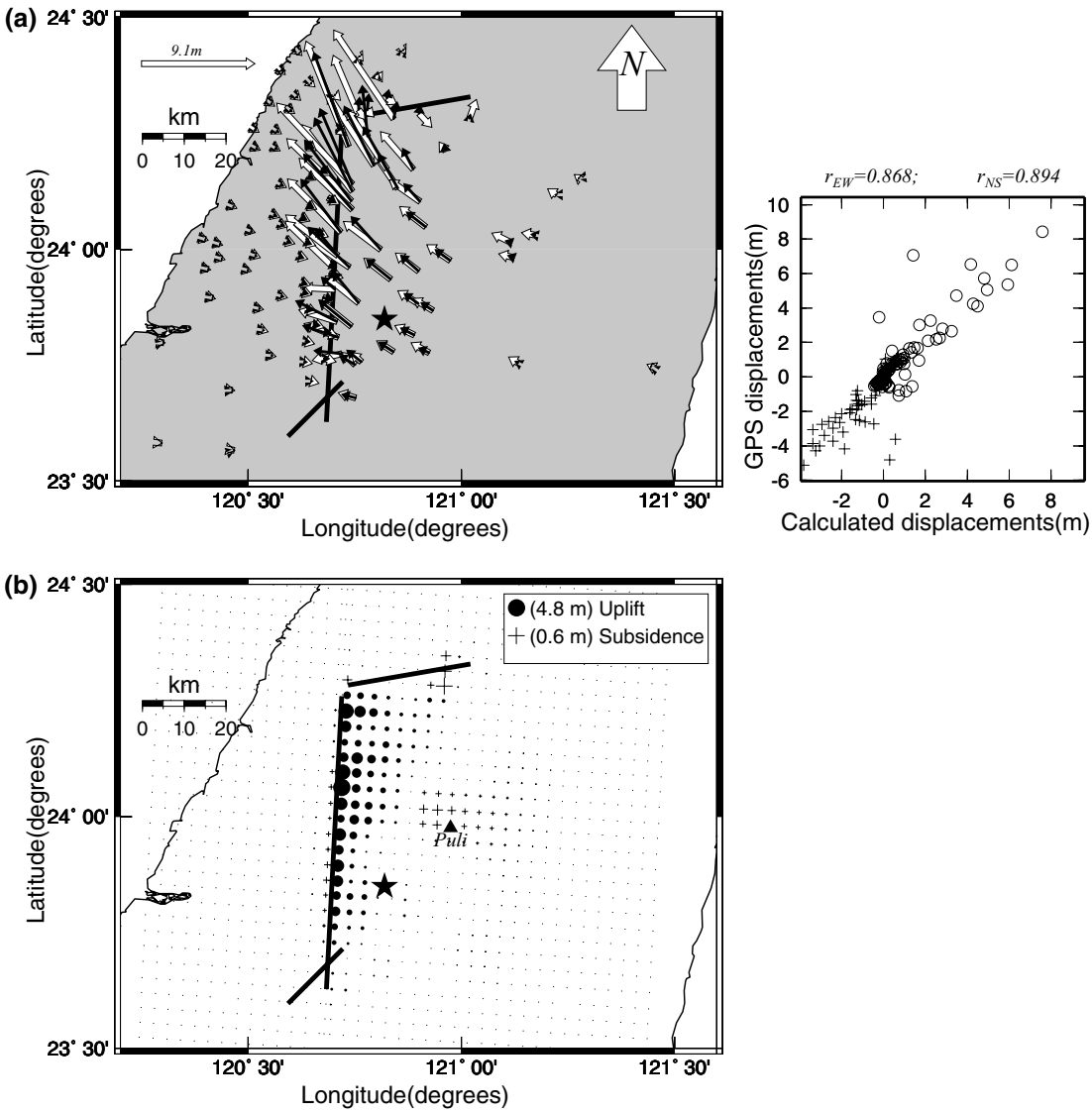

Figure 4. (a) Comparison of the calculated (black arrows) and observed GPS (white arrows) horizontal coseismic displacements (left). The correlation is good except at the northern end of the ChelungPu Fault. The scattergram of the calculated coseismic displacements and observed GPS, with the crosses and circles representing the east–west and north–south components, respectively, is on the right. The respective correlation coefficients of 0.868 and 0.894 are for the east–west and north–south components. (b) Calculated vertical coseismic displacements. The displacements decrease rapidly from west to east and become subsidence in some parts of the eastern side, which is confirmed by GPS measurement at PuLi town (solid triangle).

where A and n are constants and are determined by laboratory measurements, Q, R and T represent activation energy, gas constants and temperature (in K), respectively, and $\hat{e}$ is strain rate.

With the temperature estimated from eq. (3) and with the rheological parameters specified in the following, the effective viscosity, η, is then estimated by

$$\eta = \frac{\sigma}{2\hat{e}}, \tag{5}$$

where the deviatoric stress, σ, is given by eq. (4) and the strain rate, $\hat{e}$, is estimated from long-term GPS data. The Maxwell time, τ, then can be determined by

$$\tau = \frac{\eta}{\mu}, \tag{6}$$

where μ is rigidity.

Fig. 5 shows the distribution of the viscosities as a function of depth in the lower crust for different materials, or for the same material collected at different locations (Kirby & Kronenberg 1987, and Table 2) in dry and wet conditions with a strain rate of 1.67×10^{-6} yr^{-1}. Because the strain rate, as measured from the long-term GPS triangular network installed in central Taiwan, varies from place to place with values of $(0.03–3.32) \times 10^{-6}$ yr^{-1} (Hung *et al.* 1999), we use an average value of 1.67×10^{-6} yr^{-1} in our calculations. The lower value of viscosities occurring in the wet rheologies may reflect the strong influence of the presence of water on rock strength. Since surface deformation induced by a quake within timescales of 1 month to 10 yr causes observable deformation at the Earth's surface, this can be explained by viscous relaxation beneath the elastic crust. This result may be related to the short timescale involved in the viscoelastic relaxation process. If this is the case, 10 yr is a good least upper bound of Maxwell time for the observable deformation (Sykes *et al.* 1999). The rigidity (μ) of the Earth's crust is approximately 3×10^{10} Pa (Stein & Wysession 2003). Using eq. (6), the upper limit of viscosity is approximately 10^{19} Pa s, and was adopted by

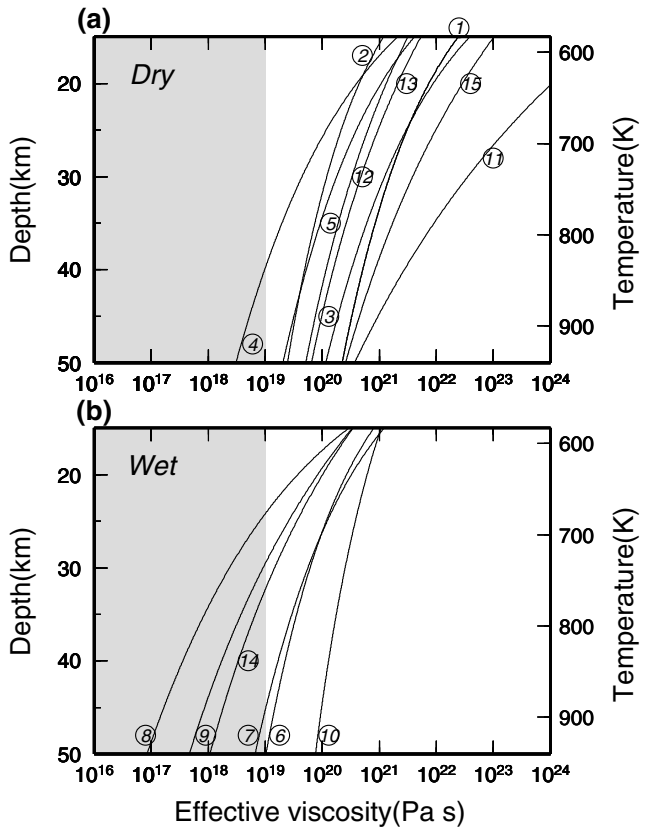

Figure 5. Viscosities of the lower crust for (a) dry and (b) wet rock-forming minerals. Each marked number corresponds to the rock-forming minerals tested in the laboratory (Kirby & Kronenberg 1987), and all are listed in Table 2. The range for the estimated viscosity lies between 10^{17} and 10^{19} Pa s.

Freed & Lin (1998). The shaded regions in Fig. 5 indicate that the range of viscosities is 10^{17}–10^{19} Pa s for the lower crust, which will be adopted for the later grid search.

The grid-search procedure is used to determine the viscosity for different models which correspond to different tectonic structures

For different earth models (models A, B and C in Fig. 3), the calculated displacements that better fit observed data is a suggestion for determining viscosity structure at the lower crust (η_c) and the upper mantle (η_m). The previous determined range of η_c (10^{17}–10^{19} Pa s) and the ratio (η_m/η_c) of 5.0×10^{-2} to 10^7 are adopted as lower and upper bounds, respectively, for grid search, which systematically varies these two parameters. For a given pair of parameters (η_m/η_c and η_c) the calculated and observed horizontal displacements are compared, and its merit function, χ^2, which is defined below (Kaufmann & Amelung 2000), is evaluated as:

$$\chi^2(\eta_k) = [O_i - P_i(\eta_k)]\left[C_{ij}^{\mathrm{d}}\right]^{-1}[O_j - P_j(\eta_k)] \tag{7}$$

where O_i and P_i ($i = 1, N$) are the ith observed and predicted horizontal displacements, respectively, η_k is the two parameters η_m and η_c and C_{ij}^{d} is the covariance matrix of the GPS data.

Since 86 per cent of the elements of the covariance matrix are zero, we assume that each GPS station is not correlated, thus the matrix becomes $C_{ij}^{\mathrm{d}} = \rho_i^2 \delta_{ij}$, where ρ_i^2 denotes variance and is estimated from GPS measurement. The root mean square (rms) is defined as

$$\varepsilon(\eta_k) = \left[\chi^2(\eta_k)/N\right]^{0.5}, \tag{8}$$

which is taken as a misfit function for the determination of η_k.

If the error in the Gaussian distribution and model parameters is complete, then the expectation value of χ^2 is N (Squires 2001) and $\varepsilon(\eta_k) = 1$. However, this is not expected in our calculation because of the uncertainty in the source rupture model and because many model parameters are not included. Therefore, $\varepsilon(\eta_k)$ is usually far larger than 1.

Figs 6(a), (b) and (c) illustrate the distribution of $\varepsilon(\eta_k)$ for the range of η_m/η_c and η_c for the three models displayed in Figs 3(a), (b) and (c), respectively, where the minimum $\varepsilon(\eta_k)$ are marked by a cross for each model. The searched η_m and η_c determined from the minimum $\varepsilon(\eta_k)$ are 5.0×10^{23} and 5.0×10^{17} Pa s, 5.0×10^{24} and 5.0×10^{17} Pa s, and 5.0×10^{23} and 5.0×10^{17} Pa s for models A, B and C, respectively, and will be used for later computations of each model. All three models in Fig. 6 reveal that the viscosity of the lower crust is 5.0×10^{17} Pa s, which correspond to a very short Maxwell time of 116 days. As stated earlier, the viscosity and the Maxwell time seem to be very low and short, but the latter is comparable

Table 2. Steady-state flow-law parameters of crustal rocks: A and n are material constants and Q is activation energy.

Code[a]	Material	A ($\mathrm{MPa}^{-n}\ \mathrm{s}^{-1}$)	n	Q ($\mathrm{kJ\ mol}^{-1}$)	Reference[b]
1	Albite rock (dry)	2.50×10^{-6}	3.9	234	1
2	Simpson quartzite (dry)	1.16×10^{-7}	2.7	134	2
3	Anorthosite (dry)	3.16×10^{-4}	3.2	238	1
4	Quartzite (dry)	1.00×10^{-3}	2.0	167	1
5	Heavitree quartzite (dry)	9.90×10^{-6}	2.4	163	3
6	Simpson quartzite (wet)	5.05×10^{-6}	2.6	145	2
7	Quartzite (wet)	1.00×10^{-4}	2.4	160	2
8	Heavitree quartzite (wet)	5.26×10^{-3}	1.4	146	3
9	Heavitree quartzite (wet)	2.91×10^{-3}	1.8	151	4
10	Heavitree quartzite (wet)	4.00×10^{-10}	4.0	135	5
11	Clinopyroxenite (dry)	15.7×10^{0}	2.6	335	1
12	Aplite (dry)	3.16×10^{-7}	3.1	163	1
13	Westerly granite (dry)	2.00×10^{-6}	3.3	186	6
14	Westerly granite (wet)	2.00×10^{-4}	1.9	140	6
15	Diabase (dry)	1.99×10^{-4}	3.4	260	1

[a]Code corresponds to curves in Fig. 5.
[b]References: (1) Shelton & Tullis (1981); (2) Koch *et al.* (1989); (3) Kronenberg & Tullis (1984); (4) Jaoul *et al.* (1984); (5) Paterson & Luan (1990); (6) Hansen & Carter (1982); (7) Schmid *et al.* (1980).

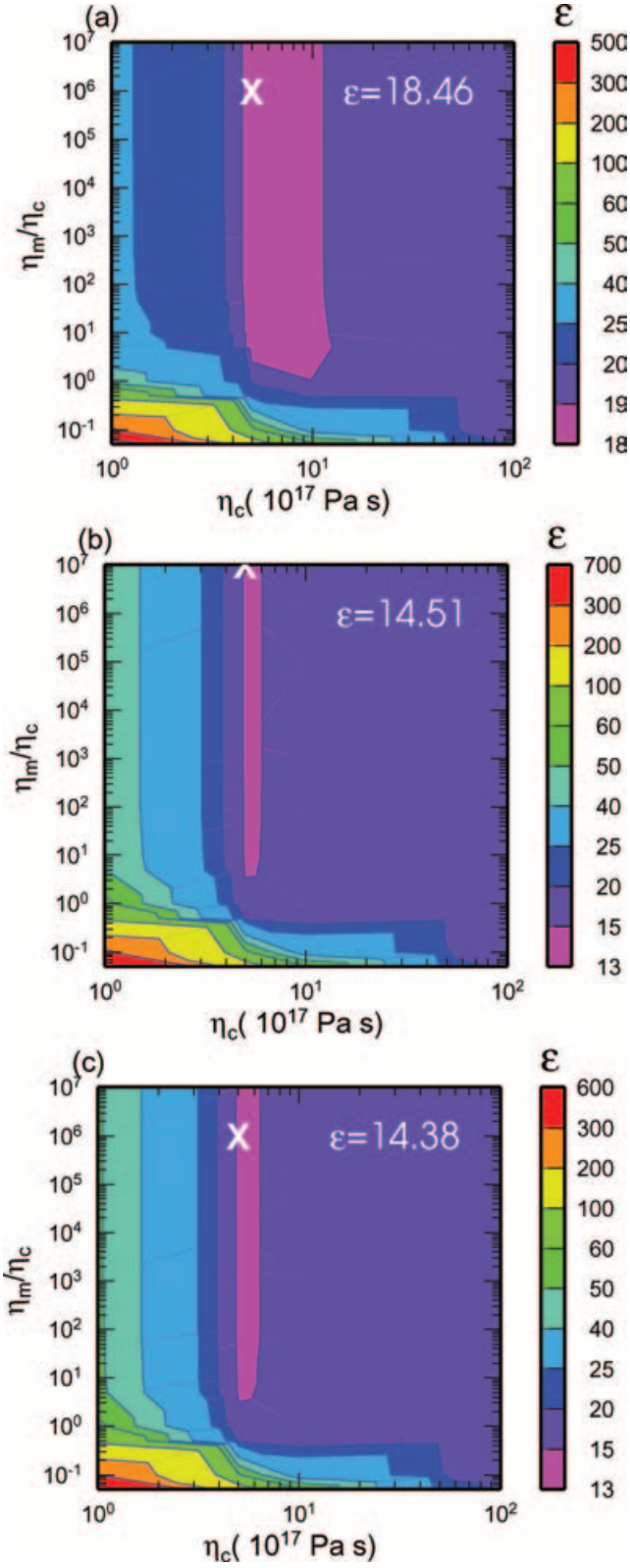

Figure 6. The root mean square (rms) of the misfit function calculated from eq. (8) by using different viscosities for lower crust, η_c, and mantle, η_m, for three models illustrated in Fig. 3: (a) for model A, (b) for model B and (c) for model C. The cross at each model denotes the minimum rms where viscosities are found.

with the result of 86 days as estimated from GPS measurements (Yu *et al.* 2001). This confirms that our estimated value of viscosity is reasonable.

6 POST-SEISMIC DEFORMATION CAUSED BY VISCOELASTIC RESPONSE

Post-seismic displacements resulting from viscoelastic relaxation in the 97-day period following the Chi-Chi event are calculated for the three models in Fig. 3, and are displayed in Fig. 7. Fig. 7(a) shows the calculated results (black arrows) for model A with $\eta_m = 5.0 \times 10^{23}$ Pa s and $\eta_c = 5.0 \times 10^{17}$ Pa s. The predicted values are generally very small, with a maximum value of 3 cm, and they are not at all comparable to the GPS measurements which have a maximum value of 14 cm. The corresponding scattergram also reveals a very low coefficient of determination, $r^2 = 22.9$ per cent (see also Table 3) for the east–west component, which definitively rules out the acceptability of model A. It should be pointed out, however, that the low predicted values using model A are not unexpected, since the base of the ChelungPu Fault does not reach the lower crust (see Fig. 3a) (Rundle & Jackson 1977).

Geological evidence supports the claim that the central mountain range was formed by the collision of the Philippine Sea Plate and the Eurasian Continental Plate, and therefore, the thickness of the lower crust beneath the range is not only greater than in western Taiwan (Wu *et al.* 1997) but also extends upwards. Model B in Fig. 3b is constructed to reflect this geological feature. The post-seismic deformation calculated from this model with $\eta_m = 5.0 \times 10^{24}$ Pa s and $\eta_c = 5.0 \times 10^{17}$ Pa s and the corresponding scattergram are illustrated in Fig. 7(b). Although the coefficient of determination, 46.0 per cent, for the east–west component is improved, it is less than 70 per cent; thus, it is not acceptable. The inconsistencies in the observed and predicted data lie mainly in the source region between the epicentre (dashed line in Fig. 7b) and the fault trace. When the data for this region are excluded from our comparison, the coefficients of determination reach 70.73 and 44.09 per cent for the east–west and north–south components, respectively. In other words, model B can be used to predict the observed data in most areas but not in the source region. Notably, the values for model B are much larger than those for model A, which supports the interpretation of Nostro *et al.* (2001) that post-seismic displacement is more significantly affected by a shallow viscoelastic layer than by a deep layer.

Fig. 7(c) shows the modelling results with $\eta_m = 5.0 \times 10^{23}$ Pa s and $\eta_c = 5.0 \times 10^{17}$ Pa s for model C, with the lower crust extending downward to 50 km. These results differ very little from those of model B (Fig. 7b) (see Table 3), which also indicates that the effect of the thickness of the viscoelastic layer is less significant in such a short time period. Although rms analysis in Fig. 6(c) for model C is slightly better than that in Fig. 6(b) for model B, the 97-day period of observed crustal evolution is too short to distinguish the viscosity structures of models B or C.

Fig. 6 indicates that the mantle viscosity can't be resolved very well from short-term GPS measurements. One may suspect that the mantle may be weaker than the lower crust. To show that it is not the case for central Taiwan, a weaker mantle with viscosity 10^{17} Pa s, which is less than the lower crust, 5.0×10^{17} Pa s, is tested for model C. The lower correlation coefficients in Fig. 8 for this model show that the calculated surface displacements do not fit the GPS measurements, especially on the western side where the predicted displacements are too large. Thus, although mantle viscosity is not

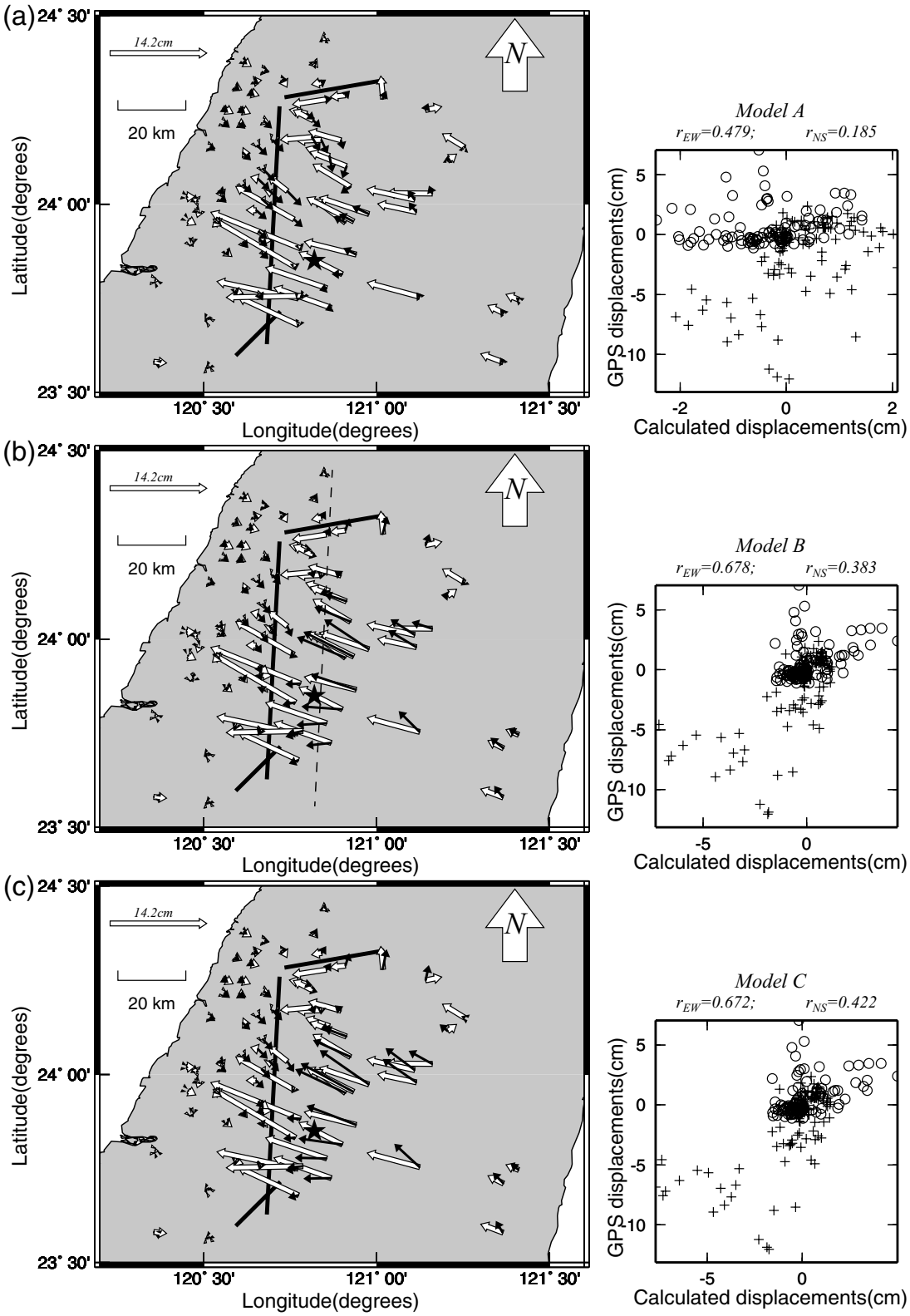

Figure 7. Comparison of the calculated (black arrows) and observed GPS (white arrows) post-seismic deformation (left) and the corresponding scattergrams (right; crosses for the east–west and circles for the north–south components) after the 97-day period following the Chi-Chi earthquake for the three different viscosity models in Figs 3 and 6. The coefficient of determination using model A (a) is very low (22.9 per cent for east–west), while those using models B (b), 46.0 per cent, and C (c), 45 per cent, are improved (see Table 3), which indicates that models B and C are more realistic than model A. However, any differences arising from using model B or C are indistinguishable in the 97-day period.

Table 3. Correlation coefficients of calculated and GPS data for different rheology models.

Models	East–west	North–south
Model A	0.479 (0.229)[a]	0.185 (0.034)
Model B	0.678 (0.460)	0.383 (0.147)
Model C	0.672 (0.452)	0.422 (0.178)
Model D	0.740 (0.548)	0.456 (0.208)
Model C + D	0.791 (0.626)	0.596 (0.355)

[a]The numbers in parentheses are the squares of the correlation coefficients (r^2). Model D, that assumes a further slip on the fault, uses an additional 2 per cent of the coseismic slip.

well resolved a weaker mantle is excluded for the areas of central Taiwan.

The results from models B and C partially support earlier reports that post-seismic deformation is due to a viscoelastic response in the lower crust. However, the fact that there are high inconsistencies in the source region (Figs 7b and c) implies that a viscoelastic response alone cannot explain the early post-seismic deformation. Consequently, we will now explore the possibility that aseismic creep may explain the remaining misfit.

7 AFTERSLIP MODEL

Although afterslip is composed of a series of discrete creep events, it can be treated as a single slip event (Marone *et al.* 1991) since most of the events occur within a short time period. Based on observations, Heki & Tamura (1997) suggested that the afterslip is differently distributed from the high-speed rupture, and the post-seismic deformation generally continues in the same direction as the initial deformation. Therefore they assume that the distribution of the short-term afterslip in the fault plane is similar to that of the coseismic slip. In considering the afterslip model, 2 per cent of the coseismic slip motion (Ji *et al.* 2001) on the fault plane is added to model C (Freed & Lin 1998), but without the viscoelastic responses, and this model is then referred to as model D. This operation is performed by calculating the coseismic displacements of 2 per cent added to the coseismic slip motion, and then the original one (Fig. 4a) is subtracted. An alternative method that includes the viscoelastic responses is to calculate the 97-day time-dependent displacements of the new model and to subtract the results in Fig. 7(c). The results using these two methods are almost identical because the viscoelastic responses resulting from that extra 2 per cent are negligible. The value of 2 per cent of coseismic slip motion is constrained by extensive modelling tests. The results calculated from the afterslip model D are displayed in Fig. 9(a). Although its coefficient of determination is better and closer to that from model C (see Table 3), the displacement patterns are quite different. The afterslip model is clearly a better predictor in the rupture areas between the epicentre and the fault trace (dashed line in Fig. 7b) but very poor for the eastern sides.

We then combine the results of the viscoelastic (Fig. 7c) and afterslip (Fig. 9a) models in Fig. 9(b). The coefficient of determination for the combined results is increased to 62.6 per cent for the east–west component and to 35.5 per cent for the north–south component (see Table 3). Even though these values fall short of the acceptable level of 70 per cent, the improvement strongly suggests that both the viscoelastic and afterslip mechanisms may concurrently have affected early post-seismic deformation in central Taiwan.

8 DISCUSSION

Our modelling of the viscoelastic response suggests that the depth of the viscosity layer has an important effect on post-seismic deformation. A model with a viscoelastic layer that does not reach the bottom of a rupture produces smaller deformations, especially in regions outside the source areas, whereas a model with a shallower viscoelastic layer produces greater deformations. The effect of the thickness of a viscoelastic layer is not significant within a 97-day period. To further investigate a possible viscoelastic response from an even shallower model, the viscoelastic layer in model C is raised 5 km closer to the surface, but its thickness is kept the same. The modelled results are shown in Fig. 10(a), where the misfits in displacements lie in the source and in the western regions, and the coefficients of determination are no better than those in Fig. 9(b). We find that viscoelastic relaxation alone is not able to predict the GPS data at an acceptable level. The combination of the viscoelastic

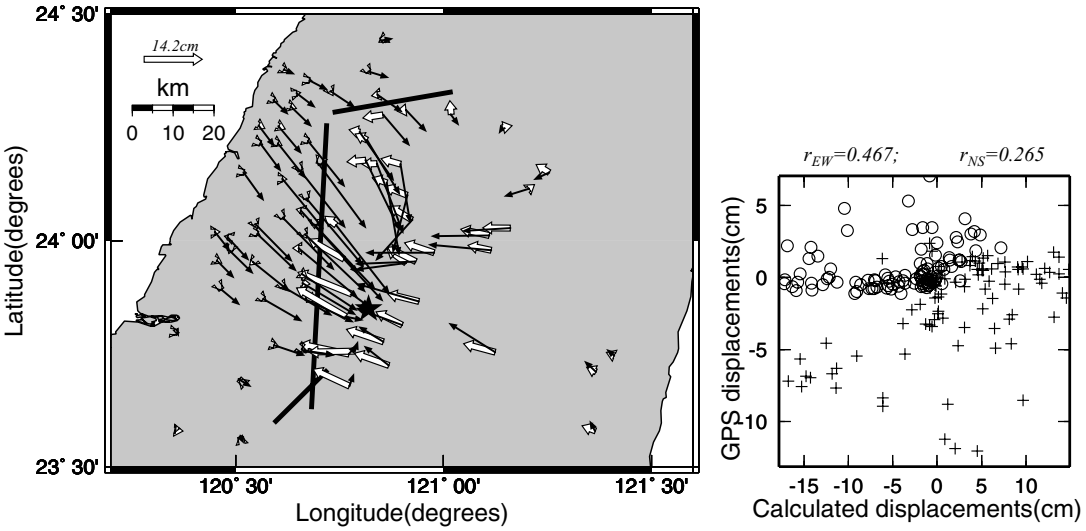

Figure 8. Results of a weaker mantle with smaller viscosity, 10^{17} Pa s, for model C. The correlation coefficients of 0.467 and 0.265 for the east–west and north–south components, respectively, are much less than that of Fig. 7(c). In addition, the predicted displacements (black arrows) are not comparable with the GPS measurements (white arrows), especially on the western side. This result indicates that a weaker mantle is not realistic in central Taiwan.

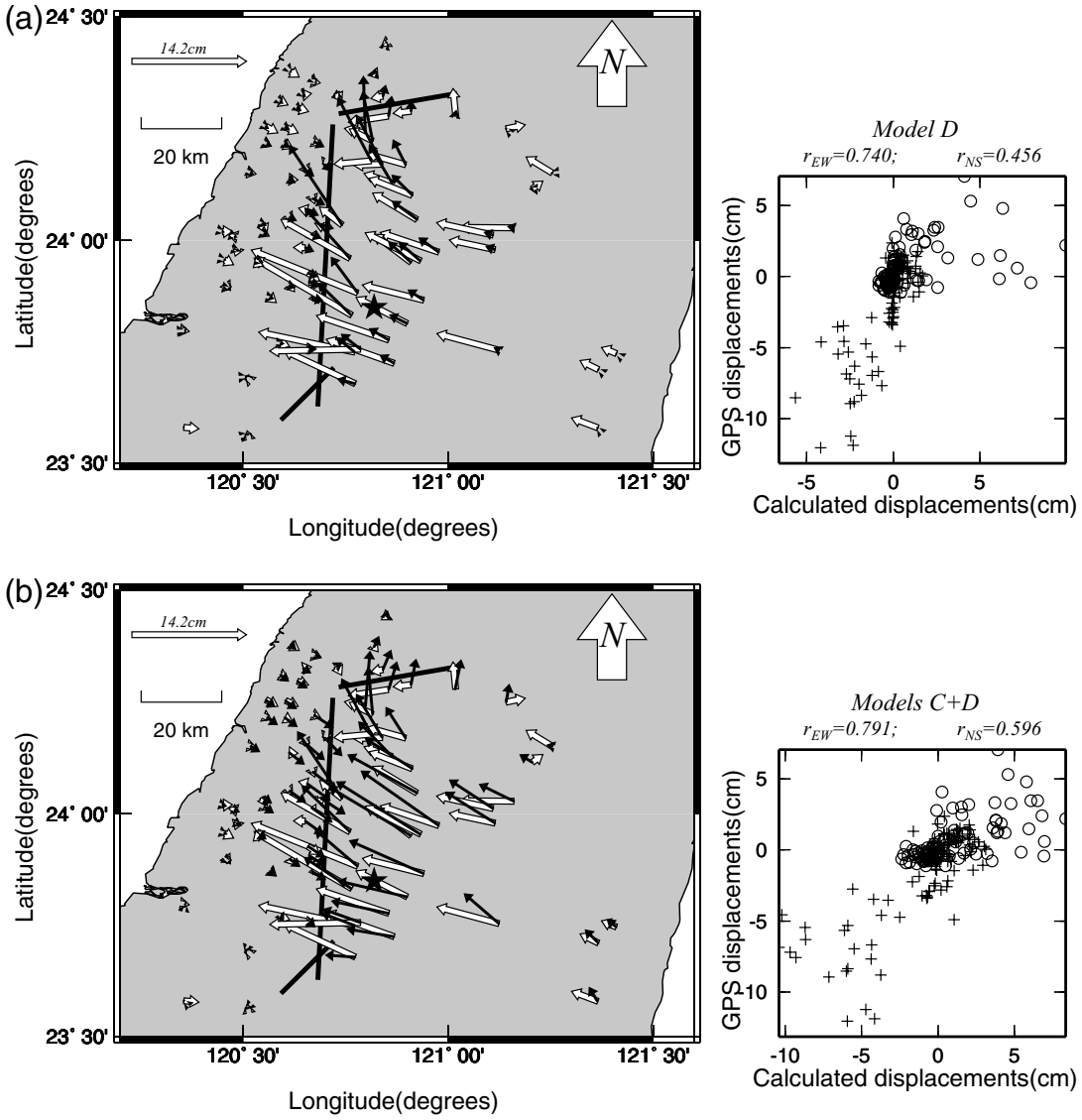

Figure 9. (a) Results from the afterslip model when 2 per cent of the source rupture slip motion of the Chi-Chi event on the fault plane is added to model C (left), and the related scattergram (right). The coefficient of determination, 54.8 per cent, for the east–west component is better than that obtained using the viscoelastic model (Figs 7b or c), but the displacement patterns are different. (b) Results from combining the viscoelastic response (Fig. 7c) and the afterslip model (left), and its scattergram (right). The improved coefficient of determination, 62.6 per cent, for the east–west component strongly suggests that both mechanisms are important.

response in Fig. 10(a) and the afterslip in Fig. 9(a) (note that it is not affected by viscosity structure) is illustrated in Fig. 10(b), where the coefficients of determination are improved but are not better than those in model C plus model D (Fig. 9b) in Table 3. Besides this, the misfits in the western regions remain. This is also an indication that too shallow a viscosity structure is unreasonable for western Taiwan.

A model that includes both a viscoelastic response and afterslip definitively results in improved predictions. Marone *et al.* (1991) pointed out that an afterslip model and the absence of seismicity above some shallow depths are related to the characteristics of velocity-strengthening and the thickness of sedimentary rocks. The aftershocks that were located on and/or within 1 km of the fault plane in the source rupture areas (not in the entire central Taiwan area) during the 97-day time period after the Chi-Chi event are plotted and shown in Fig. 11. Most early aftershocks occurred at depths below 7 km, and thus seismicity cut-off (without earthquakes) above 7 km (about the thickness of the sedimentary rocks) is clearly observed in the Chi-Chi aftershock sequence (only in the source rupture areas); in accordance with the afterslip model, this implies that the major creeping on the fault plane would have occurred at depths of less than 7 km (Marone *et al.* 1991). Based on field observations, Marone *et al.* (1991) reported that a certain amount of post-seismic creeping should normally occur on the fault plane where coseismic displacements are small and that the extent of post-seismic deformation can be used to determine the relative thickness of sediments (thicker for large post-seismic deformations and thinner for small deformations). The distribution of the source rupture model (Ji *et al.* 2001) demonstrated that at shallow depths (<8 km), the average slip motion on the northern fault plane was about 2.1 times that on the southern plane. Accordingly, the amount of post-seismic deformation should have been larger in the southern compared with that in

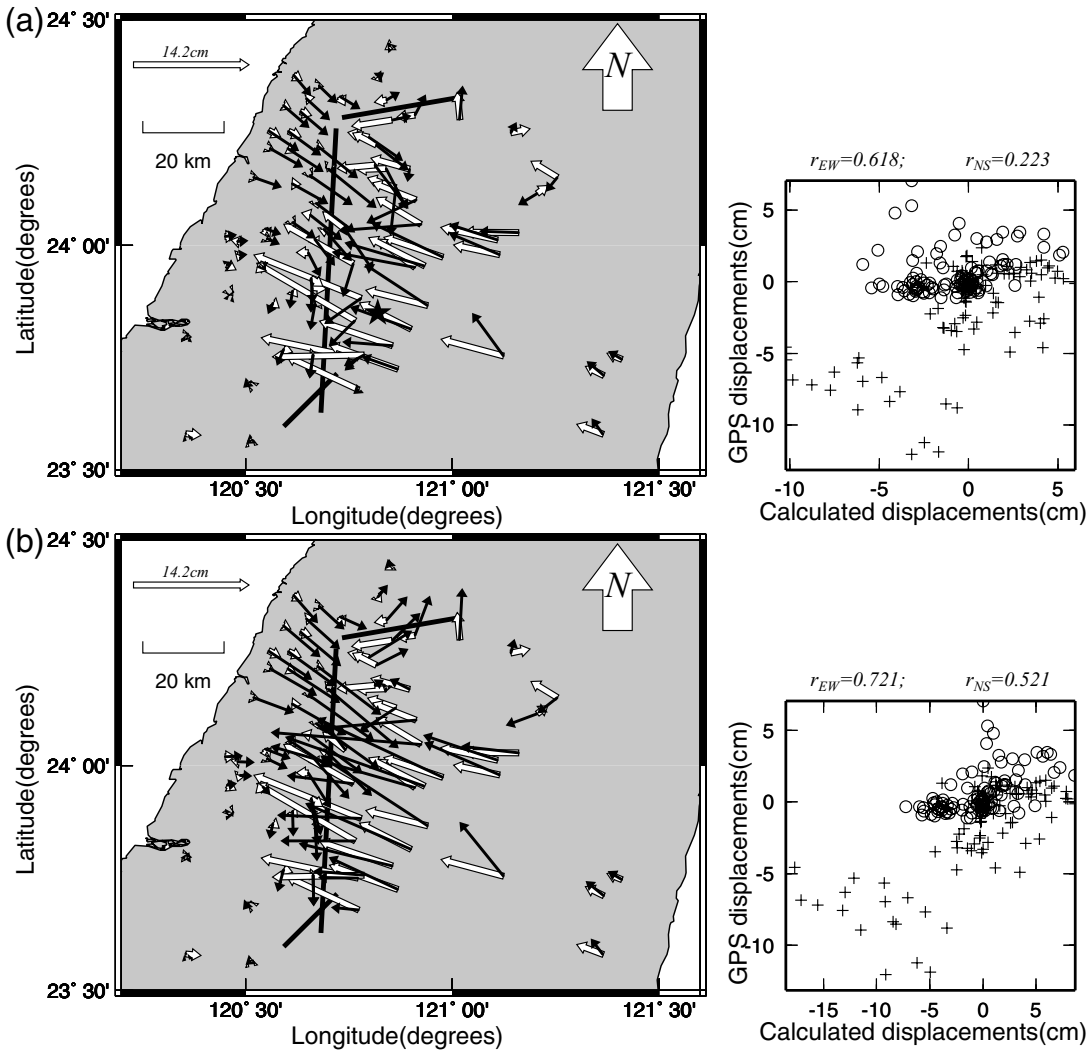

Figure 10. (a) Results from the viscoelastic response for raising the viscosity layer (model C) 5 km toward the surface, but with the same thickness (left), and its scattergram (right). The misfits in the displacements lie in the source regions and in the western regions. (b) Results from combining afterslip (Fig. 9a) (left), and its scattergram (right). The coefficients of determination for both results are no better than those in Fig. 9(b) for the east–west component. The misfits in the western regions suggest that too shallow a viscosity layer is unreasonable.

the northern parts. The results from Hsu *et al.* (2002) also show this pattern. To further identify this in the modelling, an unequal 1 per cent and 6 per cent (unlike the 2 per cent in all of the above) of the shallow coseismic slip motion above 7 km are, respectively, adjusted to the modelling of the northern and southern fault planes, and the results are illustrated in Figs 12(a) and (b) (note that the viscoelastic response is combined as well) for the horizontal and vertical component, respectively. By comparing Figs 12(a) and 9(b), it is evident that the coefficient of determination is improved from 62.6 to 72.3 per cent ($r = 0.850$) and 35.5 to 55.5 per cent ($r = 0.745$) for the east–west and north–south components, respectively. Although the true percentages of coseismic slip motion for each segment of the fault plane are not known, this improvement may support the above interpretation.

9 CONCLUSIONS

This study compares GPS data (97 days) with the results from modelling coseismic and early post-seismic deformations from the Chi-Chi earthquake. The comparisons are imperfect, but they do help us to identify plausible mechanisms of the deformations. The results firmly suggest that the afterslip dominated the post-seismic deformation in the source region, while the viscoelastic response dominated elsewhere. The combination of these two mechanisms can effectively predict data with the coefficients of determination of 72.3 and 55.5 per cent for the east–west and north–south components, respectively (Fig. 12a). The imperfect fit might be attributed to a number of factors. Among these are uncertainty in the source rupture model, an overly-simplified 2-D viscosity structure and the effect of 13 larger aftershocks (see white circles in Fig. 12a) that are not considered in the calculations.

We considered a viscoelastic response when modelling the deformations after a 97-day period because of the very short relaxation time that we estimate for central Taiwan. Since the viscoelastic response dominates long-term stress evolution, distinguishing the true model from several other possible ones to explain the 97-day GPS data may be possible when data from a larger time span become available.

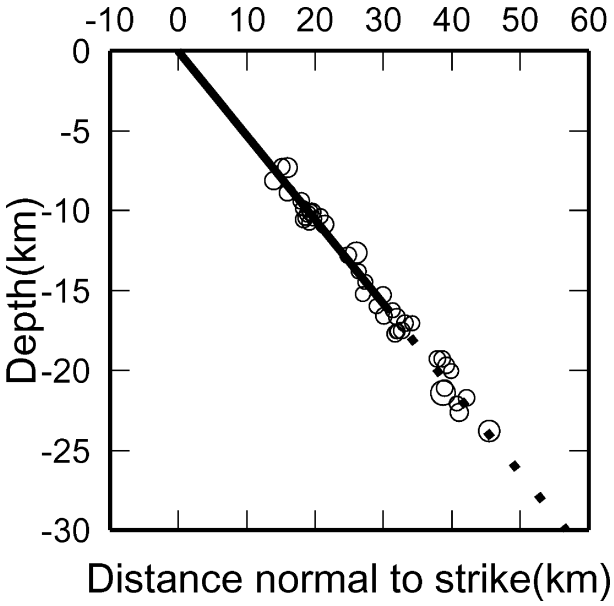

Figure 11. Aftershocks (only in the source regions) occurring on and/or near the ChelungPu fault plane (heavy line) within 3 months. A seismicity cut-off (without earthquakes) at a depth of less than 7 km is clearly observed.

ACKNOWLEDGMENTS

The authors appreciate the use of the GPS data provided by Dr S. B. Yu. Two anonymous referees provided many constructive comments, which have strengthened the quality of this manuscript. Clear-cut suggestions made by H. Schmeling, the editor, expedited our first revision. Special thanks to H. Schmeling for a very careful review and for providing many detailed comments for the second revision. The National Science Council of Taiwan R.O.C. supported this research under grant NSC 89-2921-M-194-001-EAF.

REFERENCES

Barr, T.D. & Dahlen, F.A., 1989. Brittle frictional mountain building: 2. Thermal structure and heat budget, *J. geophys. Res.,* **94,** 3923–3947.

Chase, W., 1997. *General Statistics,* John Wiley, New York.

Chinnery, M.A., 1961. The deformation of the ground around surface faults, *Bull. seism. Soc. Am.,* **51,** 355–372.

Chinnery, M.A., 1963. The stress changes that accompany strike-slip faulting, *Bull. seism. Soc. Am.,* **53,** 921–932.

Cohen, S.C., 1982. A multilayer model of time dependent deformation following an earthquake on a strike slip fault, *J. geophys. Res.,* **87,** 5409–5421.

Cohen, S.C., 1994. Evaluation of the importance of model features for cyclic deformation due to dip-slip faulting, *Geophys. J. Int.,* **119,** 831–841.

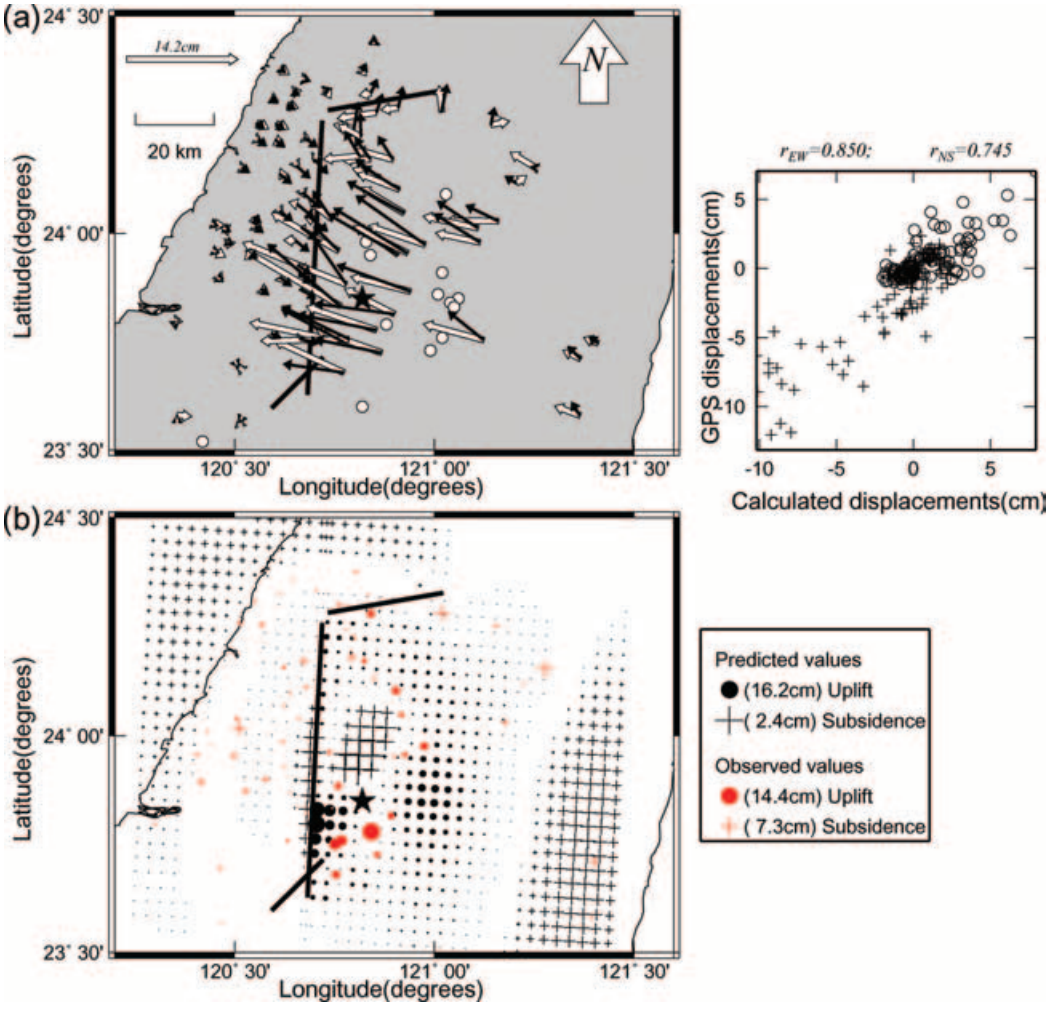

Figure 12. (a) Horizontal results when 1 and 6 per cent of the rupture slip motion of the Chi-Chi event on the northern and southern fault planes (separated by the epicentre), respectively, are added to model C (left) and its scattergram (right). Part (b) shows vertical results. The coefficient of determination reaches 72.3 per cent for the east–west component. The 13 small circles on the left of (a) stand for aftershocks with $M_L > 6.0$ that occurred within 3 months.

Cummins, P.R., Hirano, S. & Kaneda, Y., 1998. Refined coseismic displacement modeling for the 1994 Shikotan and Sanriku-oki earthquakes, *Geophys. Res. Lett.,* **25,** 3219–3222.

Deng, J., Gurnis, M., Kanamori, H. & Hauksson, E., 1998. Viscoelastic flow in the lower crust after the 1992 Landers, California, earthquake, *Science,* **282,** 1689–1692.

Deng, J., Hudnut, K., Gurnis, M. & Hauksson, E., 1999. Stress loading from viscous flow in the lower crust and triggering of aftershocks following the 1994 Northridge, California, earthquake, *Geophys. Res. Lett.,* **26,** 3209–3212.

Ergintav, S., Ergmann, R.B., McClusky, S., Cakmak, R., Reilinger, R.E., Lenk, O., Barka, A. & Zener, H., 2002. Postseismic deformation near the Izmit earthquake (17 August 1999, *M* 7.5) rupture zone, *Bull. seism. Soc. Am.,* **92,** 194–207.

Freed, A.M. & Lin, J., 1998. Time-dependent changes in failure stress following thrust earthquakes, *J. geophys. Res.,* **103,** 24 393–24 409.

Gardi, A., Cocco, M., Negredo, A.M., Sabadini, R. & Singh, S.K., 2002. Dynamic modeling of the subduction zone of central Mexico, *Geophys. J. Int.,* **143,** 809–820.

Hansen, F.D. & Carter, N.L., 1982. Creep of selected crustal rocks at 1000 MPa, *Trans. Am. Geophys. Un.,* **63,** 437.

Heki, K. & Tamura, Y., 1997. Short term afterslip in the 1994 Sanriku-Haruka-Oki earthquake, *Geophys. Res. Lett.,* **24,** 3285–3288.

Hsu, Y.J., Bechor, N., Segall, P., Yu, S.B., kuo, L.C. & Ma, K.F., 2002. Rapid afterslip following the 1999 Chi-Chi, Taiwan, earthquake, *Geophys. Res. Lett.,* **29,** doi:10.1029/2002GL014967.

Hung, J.-H., Wiltschko, D.V., Lin, H.C. & Hickman, J.B., 1999. Structure and motion of the southwestern Taiwan fold and thrust belt, *TAO,* **10,** 543–568.

Jaoul, O., Tullis, J. & Kronenberg, A., 1984. The effect of varying water contents on the creep behaviour of Heavitree quartzite, *J. geophys. Res.,* **89,** 4298–4312.

Ji, C., Helmberger, D.V., Song, T.A., Ma, K.F. & Wald, D.J., 2001. Slip distribution and tectonic implication of the 1999 Chi-Chi, Taiwan, Earthquake, *Geophys. Res. Lett.,* **28,** 4379–4382.

Kaufmann, G. & Amelung, F., 2000. Reservoir-induced deformation and continental rheology in vicinity of Lake Mead, Nevada, *J. geophys. Res.,* **105,** 16 341–16 358.

Kirby, S.H. & Kronenberg, A.K., 1987. Rheology of the lithosphere: selected topics, *Rev. Geophys.,* **25,** 1219–1244.

Koch, P.S., Christie, J.M., Ord, A. & George, R.P. Jr, 1989. Effect of water on the rheology of experimental deformed quartzite, *J. geophys. Res.,* **94,** 13 975–13 996.

Kronenberg, A.K. & Tullis, J., 1984. Flow strength of quartz aggregates: grain size and pressure effects due to hydrolytic weakening, *J. geophys. Res.,* **89,** 4281–4287.

Ma, K.F., Wang, J.H. & Zhao, D., 1996. Three-dimensional seismic velocity structure of the crust and uppermost mantle beneath Taiwan, *J. Phys. Earth.,* **44,** 85–105.

Marone, C.J., Scholz, C.H. & Bilham, R., 1991. On the mechanics of earthquake afterslip, *J. geophys. Res.,* **96,** 8441–8452.

Melosh, H.J. & Raefsky, A., 1980. The dynamic origin of subduction zone topography, *Geophys. J. R. astr. Soc.,* **60,** 333–354.

Melosh, H.J. & Raefsky, A., 1981. A simple and deficient method for introducing faults into finite element computations, *Bull. seism. Soc. Am.,* **71,** 1391–1400.

Mulargia, F. & Gasperini, P., 1995. Evaluation of the applicability of the time- and slip-predictable earthquake recurrence models to Italian seismicity, *Geophys. J. Int.,* **120,** 453–473.

Nostro, C., Piersanti, A. & Cocco, M., 2001. Normal fault interaction caused by coseismic and postseismic stress changes, *J. geophys. Res.,* **106,** 19 391–19 410.

Nur, A. & Mavko, G., 1974. Post-seismic viscoelastic rebound, *Science,* **183,** 204–206.

Okada, Y., 1985. Surface deformations due to shear and tensile faults in a half space, *Bull. seism. Soc. Am.,* **75,** 1135–1154.

Okada, Y., 1992. Internal deformation due to shear and tensile faults in a half-space, *Bull. seism. Soc. Am.,* **82,** 1018–1040.

Papazachos, C.B. & Papadimitriou, E.E., 1997. Evaluation of the global applicability of the regional time- and magnitude-predictable seismicity model, *Bull. seism. Soc. Am.,* **87,** 799–808.

Paterson, M.S. & Luan, F.C., 1990. Quartz rheology under geological conditions, in *Deformation Mechanisms, Rheology and Tectonics,* Geological Society of London Special Publication 54, pp. 299–307, eds Knipe, R.J. & Rutter, E.H., Geological Society, London.

Pollitz, F.F., Peltzer, G. & Burgmann, R., 2000. Mobility of continental mantle: evidence from postseismic geodetic observations following the 1992 Landers earthquake, *J. geophys. Res.,* **105,** 8035–8054.

Press, W.H., Teukolsky, S.A., Vetterling, W.T. & Flannery, B.P., 1992. *Numerical Recipes in C,* Cambridge University Press, New York.

Rundle, J.B. & Jackson, D.D., 1977. A kinematic viscoelastic model of the San Francisco earthquake of 1906, *Geophys. J. R. astr. Soc.,* **50,** 441–458.

Savage, J.C., 1990. Equivalent strike-slip earthquake cycles in half-space and lithosphere-asthenosphere Earth models, *J. geophys. Res.,* **95,** 4873–4879.

Sato, K., Bhatia, S.C. & Gupta, H.K., 1996. Three-dimensional numerical modeling of deformation and stress in the Himalaya and Tibetan Plateau with a simple geometry, *J. Phys. Earth,* **44,** 227–254.

Schmid, S.M., Paterson, M.S. & Boland, J.N., 1980. High temperature flow and dynamic recrystallization in Carrara marble, *Tectonophysics,* **65,** 245–280.

Shelton, G.L. & Tullis, J.A., 1981. Experimental flow laws for crustal rocks, *Trans. Am. Geophys. Un.,* **62,** 396.

Shen, Z.K., Jackson, D.D., Feng, Y., Cline, M., Kim, M., Fang, P. & Bock, Y., 1994. Postseismic deformation following the Landers Earthquake, California, 28 June 1992, *Bull. seism. Soc. Am.,* **84,** 780–791.

Squires, G.L., 2001. *Practical Physics,* Cambridge University Press, Cambridge.

Stein, S. & Wysession, M., 2003. *An Introduction to Seismology, Earthquakes, and Earth Structure,* Blackwell Publishing, Oxford.

Sykes, L.R., Shaw, B.E. & Scholz, C.H., 1999. Rethinking earthquake prediction, *Pure appl. Geophys.,* **155,** 207–232.

Thatcher, W., 1983. Nonlinear strain build-up and the earthquake cycle on the San Andreas fault, *J. geophys. Res.,* **88,** 5893–5902.

Thatcher, W. & Rundle, J.B., 1984. A viscoelastic coupling model for the cyclic deformation due to periodically repeated earthquakes at subduction zones, *J. geophys. Res.,* **89,** 7631–7640.

Tse, S.T. & Rice, J.R., 1986. Crust earthquake instability in relation to the depth variation of frictional slip properties, *J. geophys. Res.,* **91,** 9452–9472.

Turcotte, D.L. & Schubert, G., 2002. *Geodynamics,* Cambridge University Press, Cambridge.

Wahr, J. & Wyss, M., 1980. Interpretation of coseismic deformation with a viscoelastic relaxation model, *J. geophys. Res.,* **85,** 6471–6477.

Wang, J.H., 1993. *Q* values of Taiwan: a review, *J. Geol. Soc. China,* **36,** 15–24.

Wu, F.T., Rau, R.J. & Salzberg, D., 1997. Taiwan orogeny: thin-skinned or lithospheric collision?, *Tectonophysics,* **274,** 191–220.

Yen, H.Y., Yeh, Y.H. & Wu, F.T., 1998. Two-dimensional crustal structures of Taiwan from gravity data, *Tectonics,* **17,** 104–111.

Yoshioka, S., Hashimoto, M. & Hirahara, K., 1989. Displacement fields due to the 1946 Nankaido earthquake in a laterally inhomogeneous structure with the subducting Philippine Sea plate—a three-dimensional finite element approach, *Tectonophysics,* **159,** 121–136.

Yu, S.B. *et al.*, 2001. Preseismic deformation and coseismic displacements associated with the 1999 Chi-Chi, Taiwan, earthquake, *Bull. seism. Soc. Am.,* **91,** 995–1012.

Zienkiewicz, O.C., 1985. *The Finite Element Method,* McGraw-Hill, New York.